IEEE Access
Multidisciplinary | Rapid Review | Open Access Journal

Received December 22, 2017, accepted February 1, 2018, date of publication March 22, 2018, date of current version April 18, 2018.

Digital Object Identifier 10.1109/ACCESS.2018.2802778

Wideband Cross Polarization Rotation Based on Reflective Anisotropic Surfaces

MARJAN SADAT JALALI MOGHADAM, (Graduate Student Member, IEEE), MOHAMMAD AKBARI, (Student Member, IEEE), FERESHTEH SAMADI, (Student Member, IEEE), AND ABDEL-RAZIK SEBAK, (Fellow, IEEE)

Department of Electrical and Computer Engineering, Concordia University, Montréal, QC H3G2W1, Canada

Corresponding author: Marjan Sadat Jalali Moghadam (marjanjalalimoghadam@gmail.com)

ABSTRACT This paper presents a new design to broaden polarization conversion ratio (PCR) bandwidth utilizing reflective surfaces. The proposed design is based on anisotropic surfaces for linearly polarized electromagnetic waves. The combination of a traditional two-corner-cut square patch and a two-layer substrate with defected ground structure contributes to PCR bandwidth expansion and size reduction. The experimental results indicate that PCR fractional bandwidth is higher than 121% in 5.4-22 GHz band for both x- and y-polarized waves and the conversion efficiency is greater than 90%. In addition, the proposed structure is approximately robust under oblique incidences, which verifies the applicability of the structure in a practical environment. The experimental results are in excellent agreement with simulated ones. The reflective surface with wideband PCR can be utilized in various practical applications, such as radiometer, reflector antennas, remote sensors, and imaging sensors.

INDEX TERMS Anisotropic surfaces, defected ground structure, DGS, polarization conversion ratio, PCR, polarization, metasurface.

I. INTRODUCTION

Many fascinating phenomena are inherently sensitive to polarization states. Those have always been one of the key characteristics of electromagnetic (EM) waves so that extensive efforts have been made to control and manipulate them [1]–[3]. Polarization converters are generally categorized into transmission and reflection types [4]–[6]. In the transmission type, either the birefringence effect of anisotropic metamaterials or the optical activity of chiral metamaterials can be exploited. Unfortunately, traditional approaches to controlling polarization are restricted using bulky volumes. Miniature scale is required for practical purposes. Metamaterials are produced by subwavelength resonators, having unconventional EM responses that are unachievable in the natural material [7]. Hence, EM polarization states can be controlled and manipulated without any restriction using metamaterials in the sub-wavelength scale. Note that the two-dimensional metamaterials, which named metasurfaces, are utilized to attain great performance polarization convertors [7]. They have been subject to investigate experimentally and theoretically for both reflective and transmissive types of polarization convertors. Namely, a linear polarization convertor in terahertz was presented utilizing metal cut-wire array [8]. The rotation efficiency is greater than 80% because of constructive interferences. A wideband polarization conversion slab with high efficiency was earned using stacking split-ring resonators in [9]. A thin plate in quarter wave size was introduced using plasmonic metasurfaces that produce circularly polarized light in a wide frequency band in [10]. Using multi-order plasmon resonances and high impedance surfaces, wideband polarizer was shown in [11]. In [12] a particular optical polarization control is produced using the special EM resonances. However, the majority of these conventional structures function in a narrow single band or multiple separated narrow bands. PCR bandwidth expansion, high conversion efficiency, and simple design have still been shackles of designing polarizers [6]–[27].

In this article, an anisotropic surface having broadband PCR bandwidth of reflective nature and small size has been our aim. Therefore, in order to reach this goal, to expand the PCR bandwidth and miniature the periodicity of the proposed unit cell, the combination of a traditional two-corner-cut square patch of [18] and a two-layer substrate with defected

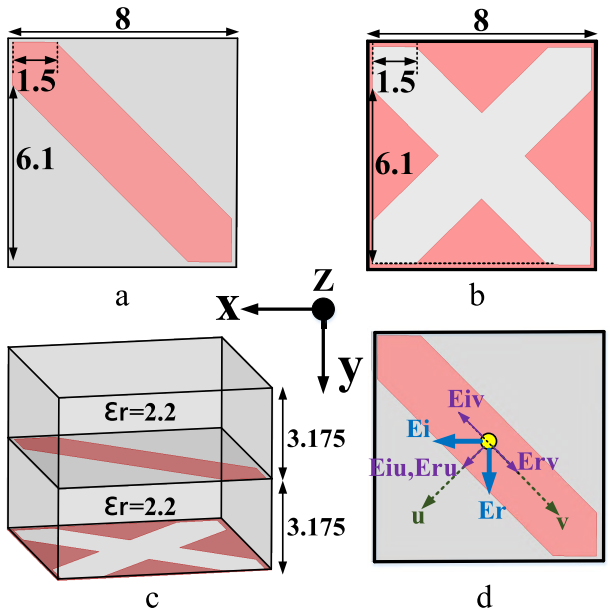

FIGURE 1. The proposed unit-cell with wideband PCR, (all dimensions are in mm), (a) top view (two-corner-cut square patch), (b) back view (DGS), (c) Side view, and (d) intuitive scheme of x -to- y polarization conversion.

ground structure (DGS) are employed, respectively. It relies on the fact that using the proposed design approaches, multiple electric and magnetic resonances are generated which results in broadening the PCR bandwidth to 120%. As compared with [18], a 20% periodicity size reduction and also 53% bandwidth enhancement with respect to a PCR efficiency of 90% or higher is achieved. Moreover, such a broad bandwidth (120%) with respect to PCR efficiency greater than 90% has never been observed in previously reported work. In order to validate the appropriate performance of the proposed reflective surfaces, PCR results under oblique incidences are determined. In addition, surface current distribution is presented to study whether the resonances generated in the unit cell are of the magnetic or electric type.

II. DESIGN OF THE STRUCTURE

A two-corner-cut square patch is used to enhance the performance of reflective cross-polarization converters.

From the geometry perspective, adding an extra 3.175 mm thick RT/duroid 5880 layer with the same characteristics (εr=2.2) along with defected ground structure (DGS) are considered as the contribution of this work. Due to the DGS, no transmission of EM wave is feasible upon incidence of the EM wave to the structure. The structure geometry is designed and optimized to broaden the PCR bandwidth and miniature the periodicity of the unit cell. Fig. 1 (a) and (b) show the geometry of the suggested unit-cell and the optimized structural parameters. The side view of the unit cell is demonstrated in Fig. 1(c). The intuitive scheme of x -to- y reflective polarization conversion is shown in Fig. 1(d). The incident electric field is decomposed into two perpendicular components u and v. Thus, the incident electric field can be expressed as $\vec{E}_i = \vec{u}E_{iu}e^{j\varphi} + \vec{v}E_{iv}e^{j\varphi}$, and the reflected electric

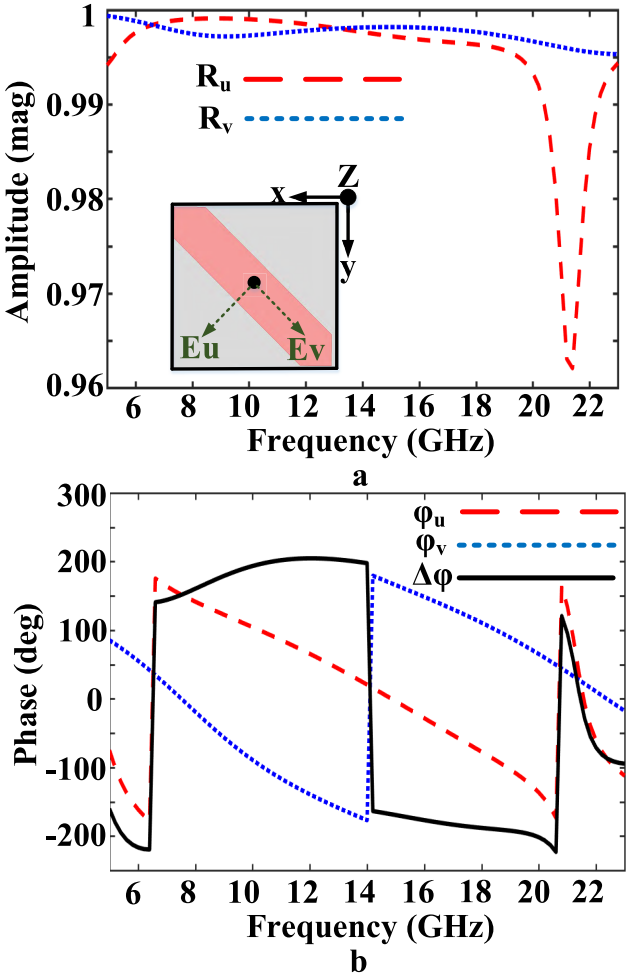

FIGURE 2. (a) Reflected amplitudes and (b) phases different illuminated with polarization along the u- and v-axis.

field as $\vec{E}_r = \vec{u}E_{ru} + \vec{v}E_{rv} = \vec{u}r_uE_{iu}e^{j\varphi} + \vec{v}r_vE_{iv}e^{j\varphi}$, where r_u and r_v are the reflected coefficients along the u- and v-axis, (see Fig. 2(a)) respectively. Due to the anisotropy property of the unit cell, a phase difference ($\Delta\phi$) exists between r_u and r_v. If $r_u \simeq r_v$ and $\Delta\varphi \simeq 180°$, the synthetic fields for Eru and Erv will be along the y-direction, as illustrated in Fig. 1d. The reflection coefficients for various polarization rotation are defined as $R_{xx} = |E_{xr}| / |E_{xi}| = \sqrt{1 + |cos\Delta\varphi/2|}$ and $R_{xy} = \frac{|E_{xr}|}{|E_{yi}|} = \sqrt{1 - |cos\Delta\varphi/2|}$, where 'E' indicates the electric field. The subscripts 'i' and 'r' denote the incidence and reflection, respectively; and the subscripts 'x' and 'y' indicate the polarization directions. Regarding above equations, when $\Delta\varphi$ is approximately $+180°$, $R_{xx} = 0$ and $R_{xy} = 1$, which verifies exactly 90° polarization conversion. With respect to Fig. 2(b), $\Delta\varphi$ is nearly $\pm180°$ ranged from 5.5 GHz to 21.5 GHz, verifying wide-band polarization rotation.

III. SIMULATED RESULTS

The suggested design, as depicted in Fig. (1), has been simulated using periodic boundary conditions in Ansys HFSS. The frequency response of co-polarized and cross-polarized

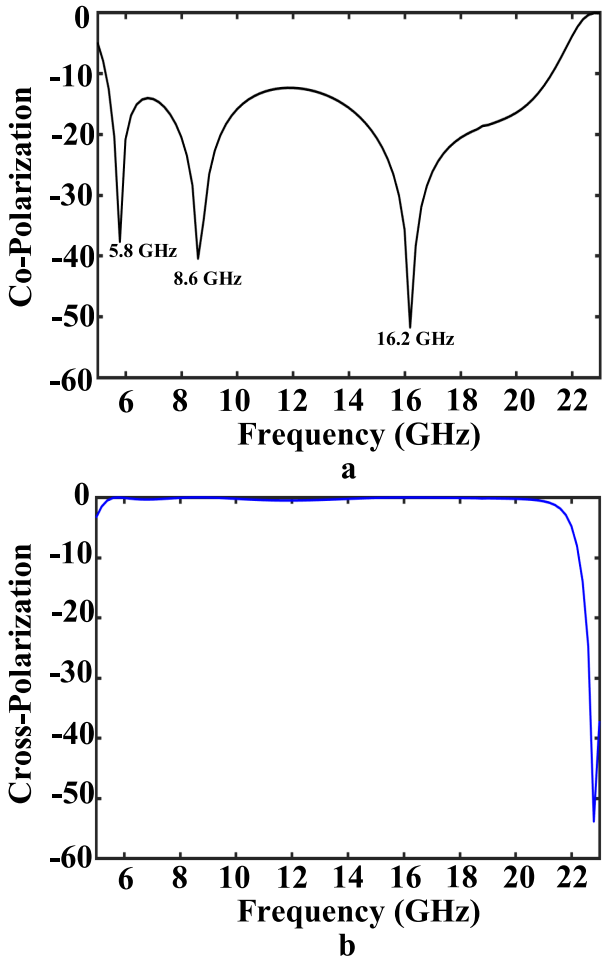

FIGURE 3. Simulated (a) co- and (b) cross-polarized reflection coefficient responses.

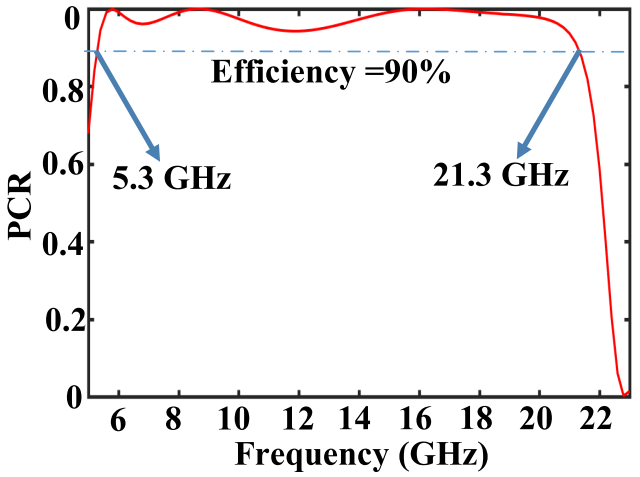

FIGURE 4. Simulated curve of PCR response (using co- and cross-polarized reflection coefficient responses obtained in Fig. 3).

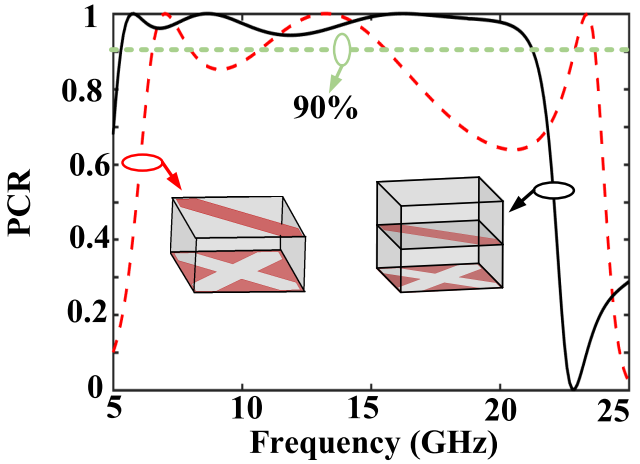

FIGURE 5. Simulated curve of PCR responses for the one-layer and two-layer unit cells.

reflection levels are attained as exhibited in Fig. 3. It is found out from Fig. 3 that co-polarized reflection component undergoes minimum values at 5.8 GHz, 8.6 GHz, and 16.2 with the respective minima of −38 dB, −41 dB, and −52 dB. The cross-polarized reflection component conserves a steady value within the desired frequency band. In this manuscript, the PCR of the structure has been subsequently computed over the frequency band from (1), in which Rxx and Rxy are co-polarized and cross-polarized reflection coefficients respectively [23].

$$PCR = \frac{R_{xy}^2}{(R_{xy}^2 + R_{xx}^2)} \tag{1}$$

The proposed anisotropic surfaces provide broadband PCR bandwidth of 15.9 GHz for the conversion efficiency is greater than 90%, ranging from 5.3 GHz to 21.2 GHz for both x- and y-polarized waves.

Moreover, this band covers considerable parts of C and K bands in addition to the perfect coverage of X and Ku bands. In the band of interest, three distinct co-polarized reflection minima combined with a maximum reflection of cross-polarized components give rise to PCR maxima (100%) at 5.8 GHz, 8.6 GHz, and 16.2 GHz respectively (see Fig. 4).

As depicted in Fig. 5, simulated curve of PCR responses for two different designs of unit cell are presented. It is quite apparent that the proposed unit cell with two layers how to improve the PCR bandwidth for an efficiency greater that 90%. Fig. 6 gives a schematic illustration of the reflection measurement method. Two horn antennae are set symmetrically with respect to the normal with a small angle of 3°. One of the antennae functions as transmitter whilst the other one as a receiver.

As shown in Fig. 6, the 90° polarization rotation of the proposed design is observed. Also, from this schematic can be realized that the reflective surfaces change the wave polarization from TM to TE and vice versa. The field distributions at the three different frequencies with maximum PCRs (5.8 GHz, 8.6 GHz, and 16.2 GHz) have been investigated to express the minimization of co-polarized reflection component of the incident EM field. In order to realize the physical

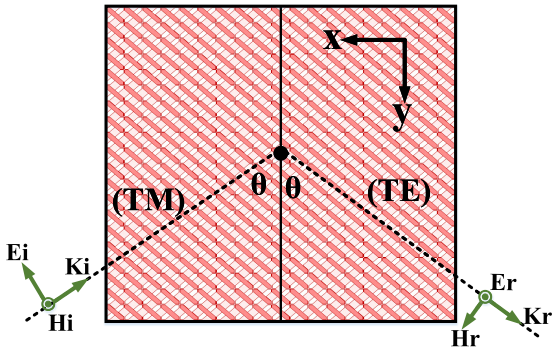

FIGURE 6. Schematic sketch of 90° polarization rotation.

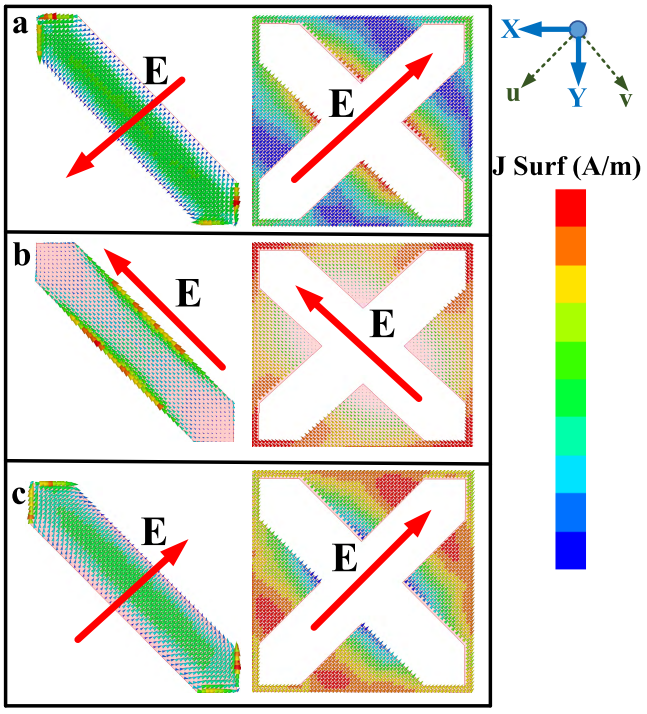

FIGURE 7. Surface current distributions on the two-corner-cut square patch and DGS at three frequencies (a) 5.8 GHz, (b) 8.6 GHz, and (c) 16.2 GHz.

mechanism of the broadband polarization rotation with the use of the suggested surface, surface current distributions on the patch and DGS are simulated at three resonances and illustrated in Fig. 7(a) to (c). It can be observed that at 5.8 GHz and 16.2 GHz, the currents flow along the u-axis. However, at 8.6 GHz, the orientation of the surface current is along the v-axis. Moreover, the surface currents along the patch at each resonance generate induced currents on the DGS.

The EM resonance types can be examined by the directions of the induced currents. As exhibited in Fig. 7(b) and Fig. 7(c), the surface currents along the patch are parallel to those induced on the DGS, which produce the electric resonance. On the contrary, with respect to Faraday's law, magnetic resonances are produced when the electric fields on the patch and DGS are anti-parallel, as shown in Fig. 7(a).

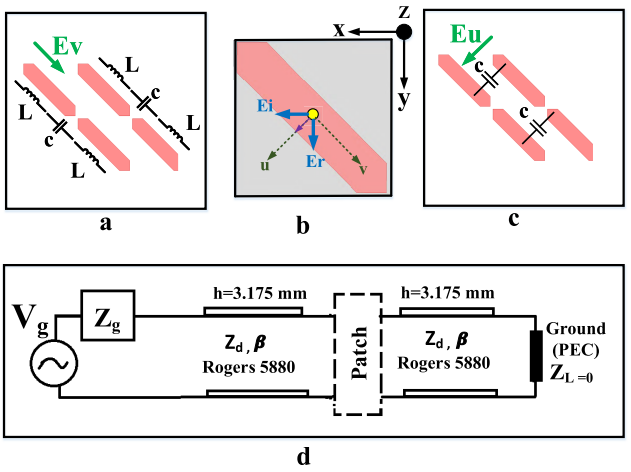

FIGURE 8. (a) Circuit model of the structure when the electric field is polarized along the v-direction, (b) intuitive scheme of x -to- y polarization conversion, and (c) circuit model of the structure when the electric field is polarized along the u-direction (Originations of the inductor and capacitor) and (d) transmission line circuit model of the unit cell.

Accordingly, at 5.8 GHz resonance, the permeability μ is very great, leading to high impedance surface ($\eta = \sqrt{\mu/\varepsilon}$), and consequently in-phase reflection. These two excitations in combination provide strong EM resonance that minimizes co-polarized reflection level at these three frequencies, thereby creating high PCR in the proposed structure. This phenomena produces wideband and high-efficiency polarization rotation. Subsequently, the impedance sheet was determined in in microscopic picture. We have regarded four vertically and horizontally unit cells once the incident field is along the v- and u-direction respectively, as depicted in Fig. 8 (a) and (c). In the former case, patches and gaps behave as inductor and capacitors respectively. In the second case, when the electric field is polarized along the u-direction, only, capacitor exist in the u direction. Those can easily be satisfied by current distribution shown in Fig. 7. Meanwhile, as exhibited in Fig. 8 (d), the two-layer unit cell can be shown in the form of a transmission line circuit model. It consists of two cascaded transmission lines with the identical lengths h=3.175 mm. The unit cell is ended to a PEC ground plate as a terminating load.

IV. RESPONSES UNDER OBLIQUE INCIDENCES

The proposed reflective design is investigated for oblique incidences under two polarizations in which the EM wave is incident on the anisotropic surfaces using the angle θ. obviously, the oblique incidence has a high effect on the polarization conversion bandwidth. Fig. 9 illustrates the simulated reflection coefficients for the two cases of co-polarization (Rxx) and cross polarization (Rxy) at various incident angles (θ). Once θ is increased from 0° to 50°, the −3-dB bandwidth of the reflection coefficient Rxy is decreased, as shown in Fig. 9 (b). At higher frequencies, Rxy fast reduces at an increment of incident angle (θ).

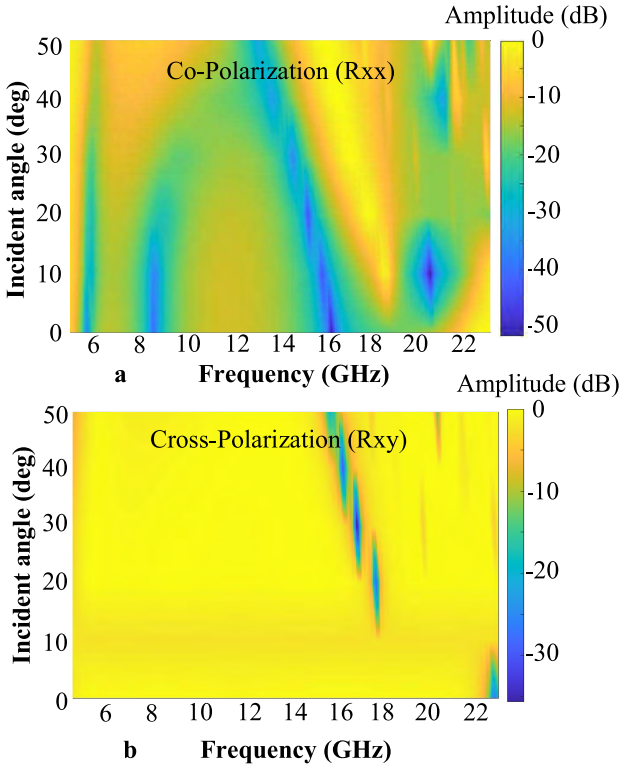

FIGURE 9. Simulated reflection coefficients of the designed polarization converter at oblique incidence of EM waves ($0° \le \theta \le 50°$) (a) Rxx and (b) Rxy.

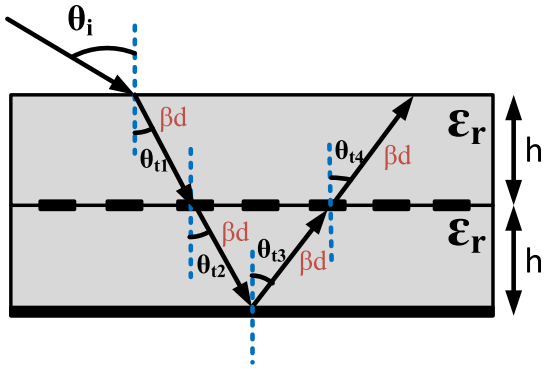

FIGURE 10. Diagrammatic illustration of EM wave propagation in a two-layer dielectric substrates at oblique incidence ($\theta_{t1} \simeq \theta_{t2} = \theta_{t3} \simeq \theta_{t4} \simeq \theta_t$).

In the case of oblique incidence, as depicted in Fig. 10, where EM waves run back and forth in a dielectric plate, the propagation phase (βd) can be indicated as

$$4\beta d = \frac{4\sqrt{\varepsilon_r}k_o h}{cos\theta_t} \tag{2}$$

Which is greater than that at the normal incidence. The additional propagation phase generates a destructive interference condition at the anisotropic surfaces and influences on the bandwidth of the cross polarization (Rxy). When incident angle (θ) is raised, the additional propagation phase varies further extremely at higher frequencies. In addition, a drop in the Rxy for oblique incidence appears at around 19 GHz, it relies on the fact that the EM energy is absorbed. This EM absorption has root in extra resonances between the DGS and traditional two-corner-cut square patch [15]. The simulated PCR result is exhibited in Fig. 11. Using [18], the polarization conversion ratio (PCR) is defined as (1). When incident angle (θ) is increased from 0° to 50°, the PCR bandwidth is reduced from 120% to 95%, with a conversion efficiency higher than 90%.

Therefore, it can be concluded that PCR is approximately independent of the incidence angle variations in the most frequency band of interest.

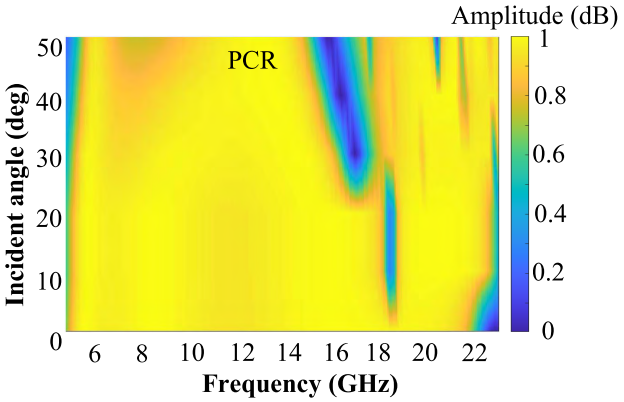

FIGURE 11. Simulation results of PCR versus incident angle and frequency.

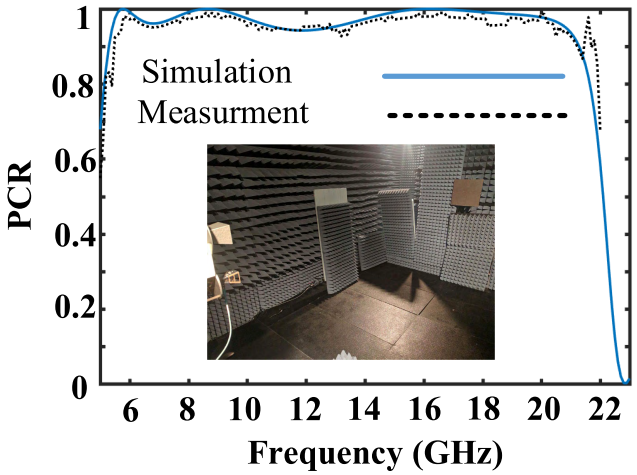

FIGURE 12. PCR results and photo of the measurement set up.

V. EXPERIMENTAL RESULTS

In order to validate the proposed design performance, a prototype of the polarizer containing 25×25 unit cells and covering an area of 200 mm × 200 mm on the top of an RT/duroid 5880 substrate with 3.175 mm thickness is fabricated and measured.

To achieve the experimental reflection coefficients, two ports of E8364B PNA network analyzer are connected to

TABLE 1. Comparison with other wideband polarization convertors.

Ref.	O. BW. (GHz)	R. BW. (%)	Electrical size (width × length × thickness)
Ref [14]	10.6-17.5	49	$0.6\lambda_g \times 0.6\lambda_g \times 0.2\lambda_g$
Ref [15]	12.4-28	77	$0.7\lambda_g \times 0.7\lambda_g \times 0.2\lambda_g$
Ref [16]	5.7-10.3	58	$0.4\lambda_g \times 0.4\lambda_g \times 0.1\lambda_g$
Ref [17]	6-17.7	98	$0.3\lambda_g \times 0.3\lambda_g \times 0.3\lambda_g$
Ref [18]	10-18.4	59	$0.6\lambda_g \times 0.6\lambda_g \times 0.2\lambda_g$
Ref [24]	14.7-18	20	$0.9\lambda_g \times 0.3\lambda_g \times 0.4\lambda_g$
Ref [25]	7390-13870	61	$0.7\lambda_g \times 0.7\lambda_g \times 0.2\lambda_g$
Proposed Design	5.4-22	121	$0.4\lambda_g \times 0.4\lambda_g \times 0.3\lambda_g$

O. BW. : Operation bandwidth (PCR ≥ 90 %)
R. BW. : Relative bandwidth (PCR ≥ 90 %)

the two linearly polarized standard-gain horn antennas in an EM anechoic chamber. The photo of the measurement set up along with the PCR results versus frequency are demonstrated in Fig. 12. One should note that another RT/duroid 5880 substrate (without any copper) with the same thickness is attached to the main design.

The PCR is more than 0.9 in a broad frequency band of 5.4 to 21.2 GHz, approximately 120% fractional bandwidth. Due to restriction on the size of the anechoic chamber and inaccuracy in the target alignment and the fabrication, the insignificant discrepancies are observed between simulation and experimental results. Table I gives a comparison between the proposed design and other reported polarization converters. The comparison indicates that the proposed reflective surface has a broadband property where the PCR is wider than 120%, implying great performance.

VI. CONCLUSION

In this paper, a new structure to expand the fractional bandwidth of polarization conversion ratio (PCR) on the reflective surface has been introduced. The combination of a traditional two-corner-cut square patch and a two-layer substrate with defected ground structure (DGS) contributes to PCR bandwidth enhancement and size miniature. The proposed structure, with expanded PCR bandwidth covering perfect X and Ku bands and main portions of C and K bands, has been designed, simulated, and experimentally validated. The experimental results show that the proposed design can rotate linearly polarized waves into their cross-polarized waves with a PCR bandwidth of nearly 120% from 5.4 GHz to 21.2 GHz for both x- and y-polarized waves with respect to a conversion efficiency higher than 90%. The reflective surface with broadband PCR can be applied in several practical applications, such as radiometer, reflector antennas, remote sensors, and imaging sensors.

ACKNOWLEDGMENT

The authors would like to thank S. Zarbakhsh and H. Abo Ghalyon of Concordia University, Canada, for his invaluable contributions during fabrication and measurements.

REFERENCES

[1] M. Akbari, M. Farahani, A.-R. Sebak, and T. A. Denidni, "*Ka*-band linear to circular polarization converter based on multilayer slab with broadband performance," *IEEE Access*, vol. 5, pp. 17927–17937, 2017.
[2] M. Akbari, H. A. Ghalyon, M. Farahani, A.-R. Sebak, and T. A. Denidni "Spatially decoupling of CP antennas based on FSS for 30-GHz MIMO systems," *IEEE Access*, vol. 5, pp. 6527–6537, 2017.
[3] M. Akbari, S. Gupta, M. Farahani, A. R. Sebak, and T. A. Denidni, "Gain enhancement of circularly polarized dielectric resonator antenna based on FSS superstrate for MMW applications," *IEEE Trans. Antennas Propag.*, vol. 16, no. 12, pp. 2324–2327, Dec. 2017.
[4] M. Farahani, J. Pourahmadazar, M. Akbari, M. Nedil, A. R. Sebak, and T. A. Denidni, "Mutual coupling reduction in millimeter-wave MIMO antenna array using a metamaterial polarization-rotator wall," *IEEE Antennas Wireless Propag. Lett.*, vol. 14, pp. 1157–1160, 2015.
[5] M. Farahani, M. Akbari, M. Nedil, A. R. Sebak, and T. A. Denidni, "Miniaturised circularly-polarised antenna with high-constitutive parameter substrate," *Electron. Lett.*, vol. 53, no. 20, pp. 1343–1344, Sep. 2017.
[6] M. Akbari, M. M. Ali, M. Farahani, A. R. Sebak, and T. Denidni, "Spatially mutual coupling reduction between CP-MIMO antennas using FSS superstrate," *Electron. Lett.*, vol. 53, no. 8, pp. 516–518, Apr. 2017.
[7] H.-Y. Chen, "Broadband perfect polarization conversion metasurfaces," *Chin. Phys. B*, vol. 24, no. 1, p. 014201, 2015.
[8] N. K. Grady *et al.*, "Terahertz metamaterials for linear polarization conversion and anomalous refraction," *Science*, vol. 359, no. 6375, p. 1235399, May 2013.
[9] Z. Wei, Y. Cao, Y. Fan, X. Yu, and H. Li, "Broadband polarization transformation via enhanced asymmetric transmission through arrays of twisted complementary split-ring resonators," *Appl. Phys. Lett.*, vol. 99, no. 22, 2011, Art. no. 221907.
[10] N. Yu, F. Aieta, P. Genevet, M. A. Kats, Z. Gaburro, and F. Capasso, "A broadband, background-free quarter-wave plate based on plasmonic metasurfaces," *Nano Lett.*, vol. 12, no. 12, pp. 6328–6333, 2012.
[11] M. Feng, J. Wang, H. Ma, W. Mo, H. Ye, and S. Qu "Broadband polarization rotator based on multi-order plasmon resonances and high impedance surfaces," *J. Appl. Phys.*, vol. 114, no. 7, p. 074508, 2013.
[12] J. Hao *et al.*, "Optical metamaterial for polarization control," *Phys. Rev. A, Gen. Phys.*, vol. 80, p. 023807, Aug. 2009.
[13] Y. Jia, Y. Liu, Y. J. Guo, K. Li, and S.-X. Gong, "Broadband polarization rotation reflective surfaces and their applications to RCS reduction," *IEEE Trans. Antennas Propag.*, vol. 64, no. 1, pp. 179–188, Jan. 2016.
[14] H. Chen *et al.*, "Ultra-wideband polarization conversion metasurfaces," in *Proc. IEEE APCAP*, Jul. 2014, pp. 1009–1011.
[15] X. Han, W.-P. Cao, H. O. Li, H. F. Ma, and T. J. Cui, "Ultra-wideband and high-efficiency linear polarization converter based on double V-shaped metasurface," *IEEE Trans. Antennas Propag.*, vol. 63, no. 8, pp. 3522–3530, Aug. 2015.
[16] J. Zhao and Y. Cheng, "A high-efficiency and broadband reflective 90° linear polarization rotator based on anisotropic metamaterial," *Appl. Phys. B*, vol. 122, no. 10, p. 255, 2016.
[17] Y. Jia, Y. Liu, Y. J. Guo, K. Li, and S. Gong, "A dual-patch polarization rotation reflective surface and its application to ultra-wideband RCS reduction," *IEEE Trans. Antennas Propag.*, vol. 65, no. 6, pp. 3291–3295, Jun. 2017.
[18] B. Q. Lin, X. Y. Da, J. L. Wu, W. Li, Y. W. Fang, and Z. H. Zhu, "Ultra-wideband and high-efficiency cross polarization converter based on anisotropic metasurface," *Miceow. Opt. Tech. Lett.*, vol. 58, no. 10, pp. 2402–2405, Oct. 2016.
[19] N. K. Grady *et al.*, "Terahertz metamaterials for linear polarization conversion and anomalous refraction," *Science*, vol. 340, no. 6138, pp. 1304–1307, 2013.
[20] J. Y. Yin, Y. Wan, Q. Zhang, and T. J. Cui, "Ultra wideband polarization-selective conversions of electromagnetic waves by metasurface under large-range incident angles," *Sci. Rep.*, vol. 5, no. 1, p. 12476, 2015.
[21] Y. Zhao and A. Alù, "Tailoring the dispersion of plasmonic nanorods to realize broadband optical meta-waveplates," *Nano Lett.*, vol. 13, no. 3, pp. 1086–1091, 2013.
[22] Y. Zhao, M. A. Belkin, and A. Alù, "Twisted optical metamaterials for planarized ultrathin broadband circular polarizers," *Nature Commun.*, vol. 3, p. 870, May 2012.
[23] X. Huang, B. Xiao, L. Guo, S. Yu, and H. Yang, "Triple-band linear and circular reflective polarizer based on E-shaped metamaterial," *J. Opt.*, vol. 16, no. 12, p. 125101, 2014.

[24] K. C. Hwang, "A novel meander-grooved polarization twist reflector," *IEEE Microw. Wireless Compon. Lett.*, vol. 20, no. 4, pp. 217–219, Apr. 2010.
[25] X. X. Zheng, Z. Y. Xiao, and X. Y. Ling, "Broadband and efficient reflective polarization converter based on a three-dimensional metamaterial," *Opt. Quantum Electron.*, vol. 48, p. 461, Sep. 2016.
[26] H. Shi, J. Li, A. Zhang, J. Wang, and Z. Xu,"Broadband cross polarization converter using plasmon hybridizations in a ring/disk cavity," *Opt. Exp.*, vol. 22, no. 17, pp. 20973–20981, 2014, doi: 10.1364/OE.22.020973.

MARJAN SADAT JALALI MOGHADAM (GS'18) received the M.Sc. degree in engineering-telecommunication from Azad University, Tehran, Iran, in 2014. She is currently pursuing the Ph.D. degree at the Electrical and Computer Engineering Department, Concordia University, Montreal, QC, Canada. Her main current research interests include millimeter wave high gain antennas, beamforming techniques, FSS, metamaterial, DRA, and polarization converters.

MOHAMMAD AKBARI (S'15) received the B.Sc. degree in engineering-telecommunication from the University of Shahid Bahonar, Kerman, Iran, in 2007, and the M.Sc. degree in electrical engineering-telecommunication from the University of Urmia, Urmia, Iran, in 2011. He is currently pursuing the Ph.D. degree with Concordia University, Montreal, QC, Canada. He has taught courses in microwave engineering, antenna theory, and fields and waves, and electromagnetic. His main field of research contains analysis and design of passive antennas, modeling of microwave structures, electromagnetic theory and analysis of UWB antennas, antenna interactions with human body, mm-wave technology, phased and switched-beam arrays, sequential feedings, periodic structures, FSS and its applications in coupling reduction, LP-to-CP polarizer, gain enhancement, bandwidth increase, RCS reduction. He has authored or co-authored approximately 80 peer-reviewed scientific journals and international conference papers. He received Graduate Concordia Merit Scholarship in 2016 and the accelerator Award in 2017.

FERESHTEH SAMADI was born in Marand, Iran, in 1990. She received the bachelor's degree (Hons.) in electrical and electronic engineering from the University of Tabriz, Iran, in 2012, the M.Sc. degree in electrical engineering from the University of Urmia, Iran, in 2014. She is currently pursuing the Ph.D. degree in electrical engineering with the University of Concordia, Montreal, QC, Canada. Her research interests include antennas and phased array antennas, scattering and beam forming and antennas for wireless communications and medical applications.

ABDEL-RAZIK SEBAK (F'10) received the B.Sc. degree (Hons.) in electrical engineering from Cairo University, Cairo, Egypt, in 1976, and the B.Sc. degree in applied mathematics from Ein Shams University, Cairo, in 1978, and the M.Eng. and Ph.D. degrees in electrical engineering from the University of Manitoba, Winnipeg, MB, Canada, in 1982 and 1984, respectively. From 1984 to 1986, he was with Canadian Marconi Company involved in the design of microstrip phased array antennas. From 1987 to 2002, he was a Professor with the Department of Electronics and Computer Engineering, University of Manitoba. He is currently a Professor with the Department of Electrical and Computer Engineering, Concordia University, Montreal, QC, Canada. His research interests include phased array antennas, millimeter-wave antennas and imaging, computational electromagnetics, and interaction of EM waves with engineered materials and bio electromagnetics. He has served as the Chair for the IEEE Canada Awards and Recognition Committee from 2002 to 2004 and as the Technical Program Chair for the 2002 IEEE CCECE Conference and the 2006 URSIANTEM Symposium. He is the Technical Program Co-Chair for the 2015 IEEE ICUWB Conference. He is a member of the Canadian National Committee of International Union of Radio Science Commission B. He was the recipient of the 2000 and 1992 University of Manitoba Merit Award for outstanding Teaching and Research, the 1994 RH Award for Outstanding Contributions to Scholarship and Research, and the 1996 Faculty of Engineering Superior.